



# A third-generation mouse model of Alzheimer's disease shows early and increased cored plaque pathology composed of wild-type human amyloid $\beta$ peptide

Received for publication, June 11, 2021, and in revised form, July 15, 2021. Published, Papers in Press, July 27, 2021.

<https://doi.org/10.1016/j.jbc.2021.101004>

Kaori Sato<sup>1,2,‡</sup>, Naoto Watamura<sup>1,‡</sup>, Ryo Fujioka<sup>1</sup>, Naomi Mihira<sup>1</sup>, Misaki Sekiguchi<sup>1</sup>, Kenichi Nagata<sup>3</sup>, Toshio Ohshima<sup>2</sup>, Takashi Saito<sup>4</sup>, Takaomi C. Saïdo<sup>1,\*</sup> , and Hiroki Sasaguri<sup>1,\*</sup> 

From the <sup>1</sup>Laboratory for Proteolytic Neuroscience, RIKEN Center for Brain Science, Wako, Saitama, Japan; <sup>2</sup>Laboratory for Molecular Brain Science, Department of Life Science and Medical Bioscience, Waseda University, Shinjuku, Tokyo, Japan; <sup>3</sup>Department of Functional Anatomy and Neuroscience, Nagoya University Graduate School of Medicine, Nagoya, Aichi, Japan; and <sup>4</sup>Department of Neurocognitive Science, Institute of Brain Science, Nagoya City University Graduate School of Medical Sciences, Nagoya, Aichi, Japan

Edited by Paul Fraser

We previously developed single *App* knock-in mouse models of Alzheimer's disease (AD) harboring the Swedish and Beyreuther/Iberian mutations with or without the Arctic mutation (*App*<sup>NL-G-F</sup> and *App*<sup>NL-F</sup> mice, respectively). These models showed A $\beta$  pathology, neuroinflammation, and cognitive impairment in an age-dependent manner. The former model exhibits extensive pathology as early as 6 months, but is unsuitable for investigating A $\beta$  metabolism and clearance because the Arctic mutation renders A $\beta$  resistant to proteolytic degradation and prone to aggregation. In particular, it is inapplicable to preclinical immunotherapy studies due to its discrete affinity for anti-A $\beta$  antibodies. The latter model may take as long as 18 months for the pathology to become prominent, which leaves an unfulfilled need for an Alzheimer's disease animal model that is both swift to show pathology and useful for antibody therapy. We thus utilized mutant *Psen1* knock-in mice into which a pathogenic mutation (P117L) had been introduced to generate a new model that exhibits early deposition of wild-type human A $\beta$  by crossbreeding the *App*<sup>NL-F</sup> line with the *Psen1*<sup>P117L/WT</sup> line. We show that the effects of the pathogenic mutations in the *App* and *Psen1* genes are additive or synergistic. This new third-generation mouse model showed more cored plaque pathology and neuroinflammation than *App*<sup>NL-G-F</sup> mice and will help accelerate the development of disease-modifying therapies to treat preclinical AD.

The major pathological hallmark of Alzheimer's disease (AD), the most common type of dementia, is deposition of amyloid  $\beta$  peptide (A $\beta$ ) in the brain (1, 2). Over 300 mutations in the *presenilin 1* (*PSEN1*) and *presenilin 2* (*PSEN2*) genes and more than 50 mutations in the *amyloid precursor protein* (*APP*) gene have been identified as disease-associated mutations (Alzforum, <http://www.alzforum.org>). These findings

have led to the development of transgenic mice overexpressing mutant APP or APP/PSEN1 cDNAs (first-generation models) (3). Such mouse models, however, often suffer from experimental limitations caused by overproduction of APP fragments such as C-terminal fragment of APP generated by  $\beta$ -secretase ( $\beta$ -CTF) and APP intracellular domain (AICD), both of which do not appear to accumulate in AD brains and may induce artificial endosomal abnormalities (4) and transcriptional malfunctions (5), respectively. Other overexpression artifacts include calpain activation (6), calpastatin-deficiency-induced early lethality (7), and endoplasmic reticulum stresses (8). In addition, Gamache *et al.* (9) demonstrated that the random insertion of transgene(s) destroyed unexpectedly large regions in endogenous gene loci of the host animal. We suggest that all transgenic models overexpressing APP or APP/PSEN1 that are being used in research should be subjected to whole genome sequencing to identify the destroyed loci that may have affected their phenotypes.

To overcome these drawbacks, we previously generated *App*<sup>NL-G-F/NL-G-F</sup> knock-in (*App*<sup>NL-G-F</sup>) and *App*<sup>NL-F/NL-F</sup> knock-in (*App*<sup>NL-F</sup>) mice that harbor the Swedish (KM670/671NL) (10) and Beyreuther/Iberian (I716F) (11) mutations with or without the Arctic (E693G) (12) mutation (second-generation models) (3, 13). These mice showed typical A $\beta$  pathology, neuroinflammation, and memory impairment (13, 14) and are being used by more than 500 research groups worldwide. Thus far, the *App*<sup>NL-G-F</sup> line has been more frequently used than the *App*<sup>NL-F</sup> line because the former develops A $\beta$  pathology approximately three times faster than the latter (13) and can be conveniently used to analyze downstream events such as neuroinflammation (15–17), pericyte signaling (18), oxidative stress (19–21), tau propagation (22), and spatial memory impairment (14, 23, 24).

However, the *App*<sup>NL-G-F</sup> line is unsuitable for investigating A $\beta$  metabolism, clearance, and deposition because the Arctic mutation present in the middle of A $\beta$  sequence renders A $\beta$  resistant to proteolytic degradation (25) and prone to aggregation (12). In particular, it is unsuitable for use in preclinical

<sup>‡</sup> These authors contributed equally to this work.

\* For correspondence: Takaomi C. Saïdo, [takaomi.saido@riken.jp](mailto:takaomi.saido@riken.jp); Hiroki Sasaguri, [hiroki.sasaguri@riken.jp](mailto:hiroki.sasaguri@riken.jp).

studies of immunotherapy due to its discrete affinity for anti-A $\beta$  antibodies even in the presence of guanidine hydrochloride (GuHCl) (13). The Arctic mutation may also interfere with the direct or indirect interactions between A $\beta$  deposition and apolipoprotein E genotype (26) although there is no experimental evidence. In contrast, the *App*<sup>NL-F</sup> line does accumulate wild-type human A $\beta$ , but it takes as long as approximately 18 months for the pathology to become prominent (13); 18 months are too long for researchers to wait in pragmatic terms. The aim of the present study was thus to generate a new mouse model that accumulates wild-type human A $\beta$  as quickly as the *App*<sup>NL-G-F</sup> model, but without depending on the Arctic mutation.

We devised the strategy to utilize the heterozygous *Psen1*<sup>P117L/WT</sup> mutant line (*Psen1*<sup>P117L</sup>) that exhibited the largest increase in A $\beta$ <sub>42</sub>/A $\beta$ <sub>40</sub> ratio in the brain among several *Psen1* mutants that we generated (27). In the present study, we attempted to crossbreed *App*<sup>NL-F</sup> mice with *Psen1*<sup>P117L</sup> mice despite it being unclear whether their pathogenic effects, both of which act on the  $\gamma$ -cleavage of  $\beta$ -CTF, are additive or not *in vivo*. We demonstrate here that the *Psen1*<sup>P117L</sup> mutation markedly enhances the pathological phenotypes of *App*<sup>NL-F</sup> mice additively or synergistically. We anticipate that these double mutant mice (third-generation model) will become highly relevant tools for examining the mechanisms upstream of A $\beta$  deposition and for preclinical screening of disease-modifying therapy candidates, which, for instance, promote A $\beta$  degradation or disaggregation, without any concern regarding the artificial effect of the Arctic mutation.

## Results

### *App*<sup>NL-F</sup>*Psen1*<sup>P117L</sup> double-mutant mice produce higher levels of A $\beta$ <sub>42</sub> than *App*<sup>NL-F</sup> mice

To analyze the combined effect of *App* and *Psen1* mutations on amyloid pathology *in vivo*, we first prepared *App*  $\times$  *Psen1* double-mutant mice carrying mutations in the endogenous genes. We crossbred *Psen1*<sup>P117L</sup> mice (27), produced by using cytosine base editors (28), with *App*<sup>NL-F</sup> mice (13) to generate *App*<sup>NL-F/NL-F</sup>  $\times$  *Psen1*<sup>P117L/WT</sup> double-mutant mice (*App*<sup>NL-F</sup>*Psen1*<sup>P117L</sup> mice). It should be noted that the double-mutant mice used in our experiments were heterozygous for the *Psen1* mutation.

*App*<sup>NL-F</sup> and *App*<sup>NL-F</sup>*Psen1*<sup>P117L</sup> mice expressed indistinguishable quantities of APP and  $\alpha/\beta$ -CTFs (Fig. 1A), suggesting that the P117L mutation does not alter processing of APP by  $\alpha$  and  $\beta$  secretases. Consistent with our previous report (13), the Swedish mutations increased the ratio of  $\beta/\alpha$ -CTFs to an identical extent in both lines. We then quantified A $\beta$ <sub>40</sub> and A $\beta$ <sub>42</sub> levels in the cortices of *App*<sup>NL-F</sup> and *App*<sup>NL-F</sup>*Psen1*<sup>P117L</sup> mice by Enzyme-Linked Immunosorbent Assay (ELISA). At 3 months of age, male *App*<sup>NL-F</sup>*Psen1*<sup>P117L</sup> mice produced 22.5-fold GuHCl-soluble (Tris-insoluble) A $\beta$ <sub>42</sub> compared with *App*<sup>NL-F</sup> mice (Fig. 1B): female samples showed a similar (26.2-fold) increase. The increase of A $\beta$ <sub>40</sub> was much smaller, resulting in approximately 11-fold elevation in the A $\beta$ <sub>42</sub>/A $\beta$ <sub>40</sub>

ratio of male *App*<sup>NL-F</sup>*Psen1*<sup>P117L</sup> mice compared with *App*<sup>NL-F</sup> mice (Fig. 1B). Female mice showed a similar tendency. In 12-month-old *App*<sup>NL-F</sup>*Psen1*<sup>P117L</sup> mice, the quantity of A $\beta$ <sub>42</sub> increased considerably in both Tris-soluble and GuHCl-soluble fractions (Fig. 1, C and D). Given that the 3-month-old single *Psen1*<sup>P117L</sup> mice showed only a 2- to 3-fold increase in A $\beta$ <sub>42</sub> production compared with wild-type controls (27), our data indicate that the combination of the *App*<sup>NL-F</sup> and *Psen1*<sup>P117L</sup> mutations acts on the  $\gamma$ -secretase activity in an additive or synergistic manner.

### The *Psen1*<sup>P117L</sup> mutation also influences A $\beta$ <sub>43</sub> production

We previously reported that A $\beta$ <sub>43</sub> is as pathogenic as A $\beta$ <sub>42</sub> (29). We thus performed A $\beta$ <sub>43</sub> ELISA on cortices from 3- and 12-month-old *App*<sup>NL-F</sup> and *App*<sup>NL-F</sup>*Psen1*<sup>P117L</sup> mice. The Tris-soluble, but not insoluble, A $\beta$ <sub>43</sub> increased more than 2-fold in the brains of *App*<sup>NL-F</sup>*Psen1*<sup>P117L</sup> mice at 3 months of age compared with *App*<sup>NL-F</sup> mice (Fig. 2, A and B). Because we treat the “soluble” fractions with GuHCl before the ELISA measurement (30), soluble oligomers are likely included in these fractions. A $\beta$ <sub>43</sub> levels in the GuHCl fractions increased with aging in both *App*<sup>NL-F</sup> and *App*<sup>NL-F</sup>*Psen1*<sup>P117L</sup> mice (Fig. 2C). Some *Psen1* mutations such as I213T and R278I result in the overproduction of A $\beta$ <sub>43</sub> *in vivo* (29, 31). It is possible that P117L alone or combination with Swedish/Iberian mutations in the *App* gene may lead to an increase in A $\beta$ <sub>43</sub> by modifying the carboxypeptidase-like activity of  $\gamma$ -secretase in the brain (32, 33). Intriguingly, the A $\beta$ <sub>43</sub> pathology became more prominent with aging. (See below.)

### A $\beta$ deposition starts as early as 3 months of age in *App*<sup>NL-F</sup>*Psen1*<sup>P117L</sup> mice

We next examined A $\beta$  pathology in the brains of *App*<sup>NL-F</sup>*Psen1*<sup>P117L</sup> mice. Immunofluorescence analyses detected A $\beta$  plaques in the cortices of *App*<sup>NL-F</sup>*Psen1*<sup>P117L</sup> mice at 3 months of age (Fig. 3, A and B), whereas *App*<sup>NL-F</sup> mice took as long as 6 months to reach an initial and minimal deposition of A $\beta$  (13). At 12 months, *App*<sup>NL-F</sup>*Psen1*<sup>P117L</sup> mice displayed prominent amyloidosis in the cortex and hippocampus comparable with that of *App*<sup>NL-G-F</sup> mice, while significantly fewer A $\beta$  plaques were observed in *App*<sup>NL-F</sup> mice (Fig. 3, A–C). Of note, the number of subcortical plaques in *App*<sup>NL-F</sup>*Psen1*<sup>P117L</sup> mice was significantly less than that in *App*<sup>NL-G-F</sup> mice, implying that *App*<sup>NL-F</sup>*Psen1*<sup>P117L</sup> mice may recapitulate the human pathology in a more faithful manner (34). *App*<sup>NL-F</sup>*Psen1*<sup>P117L</sup> mice produced dominant deposition of A $\beta$ <sub>42</sub> with minimal A $\beta$ <sub>40</sub> (Fig. 3D), which is consistent with observations made on *App*<sup>NL-F</sup> and *App*<sup>NL-G-F</sup> mice and human samples (13). Remarkably, we detected a significantly larger number of A $\beta$ <sub>43</sub>-positive plaques in the cortical, hippocampus, and subcortical regions of *App*<sup>NL-F</sup>*Psen1*<sup>P117L</sup> mice than in those regions of *App*<sup>NL-F</sup> and *App*<sup>NL-G-F</sup> mice (Fig. 3, D and E). These results imply that the Swedish/Iberian and P117L mutations together may accelerate the generation of longer A $\beta$  species including A $\beta$ <sub>42</sub> and A $\beta$ <sub>43</sub>, resulting in A $\beta$  pathology at younger ages.

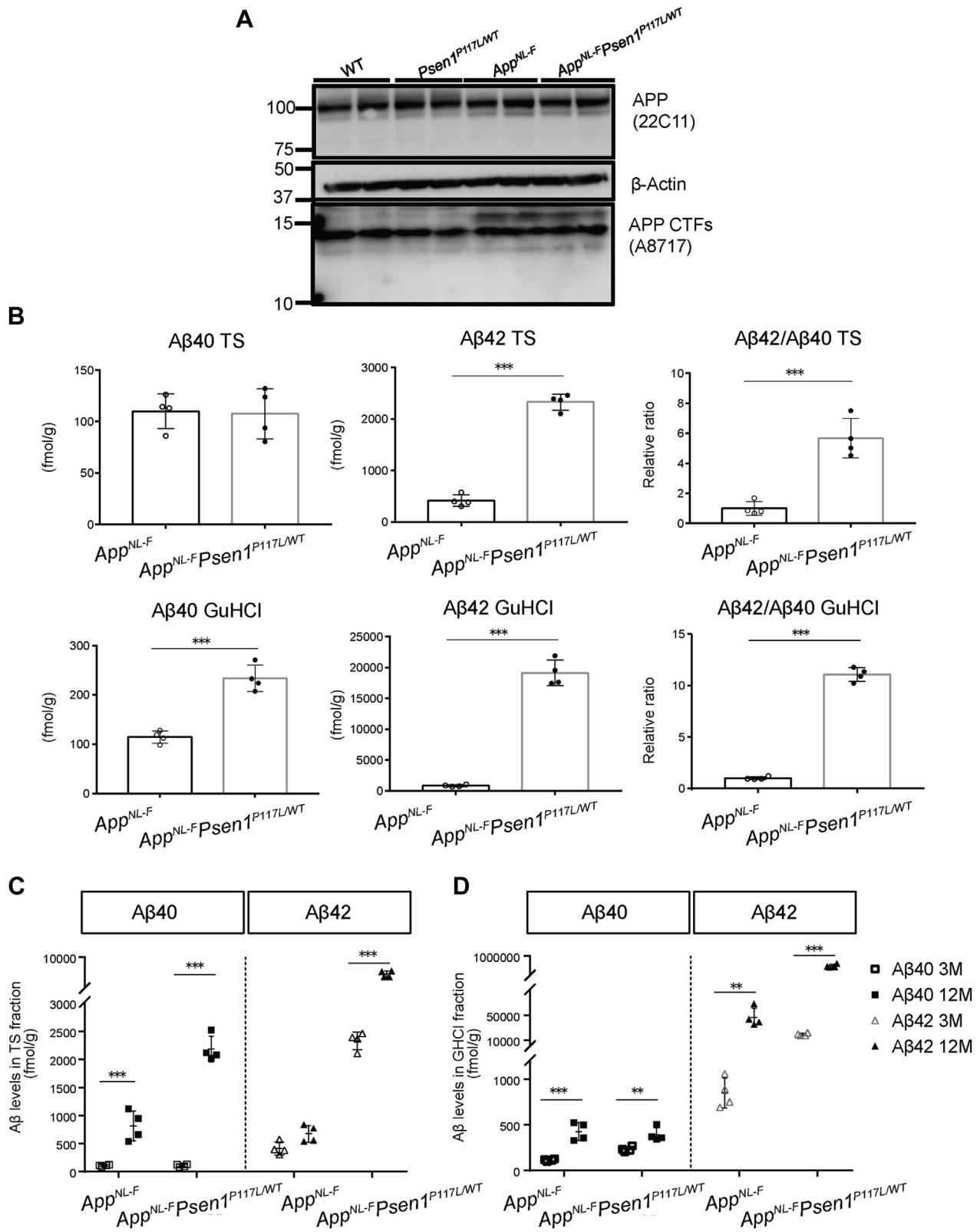


**Figure 1. APP processing and A $\beta$ <sub>40</sub> and A $\beta$ <sub>42</sub> production in the brains of *App<sup>NL-F</sup>Psen1<sup>P117L</sup>* mice.** A, APP processing in the cortices of WT, *Psen1<sup>P117L</sup>*, *App<sup>NL-F</sup>*, and *App<sup>NL-F</sup>Psen1<sup>P117L</sup>* mice. Full blot images of western blotting are shown in [Figure S1](#) (CTF) and [Figure S2](#) (APP). B, A $\beta$ <sub>40</sub> and A $\beta$ <sub>42</sub> detected by ELISA from the cortices of 3-month-old *App<sup>NL-F</sup>* and *App<sup>NL-F</sup>Psen1<sup>P117L</sup>* mice. *App<sup>NL-F</sup>* (n = 4) and *App<sup>NL-F</sup>Psen1<sup>P117L</sup>* (n = 4) (Student's t test). C and D, A $\beta$ <sub>40</sub> and A $\beta$ <sub>42</sub> using Tris-HCl (C) and GuHCl (D) soluble fractions from 3- and 12-month-old mice. *App<sup>NL-F</sup>* (n = 4) and *App<sup>NL-F</sup>Psen1<sup>P117L</sup>* (n = 4) (two-way ANOVA followed by Sidak's multiple comparisons test). Each bar represents the mean  $\pm$  SD. \**p* < 0.05, \*\**p* < 0.01, \*\*\**p* < 0.001.

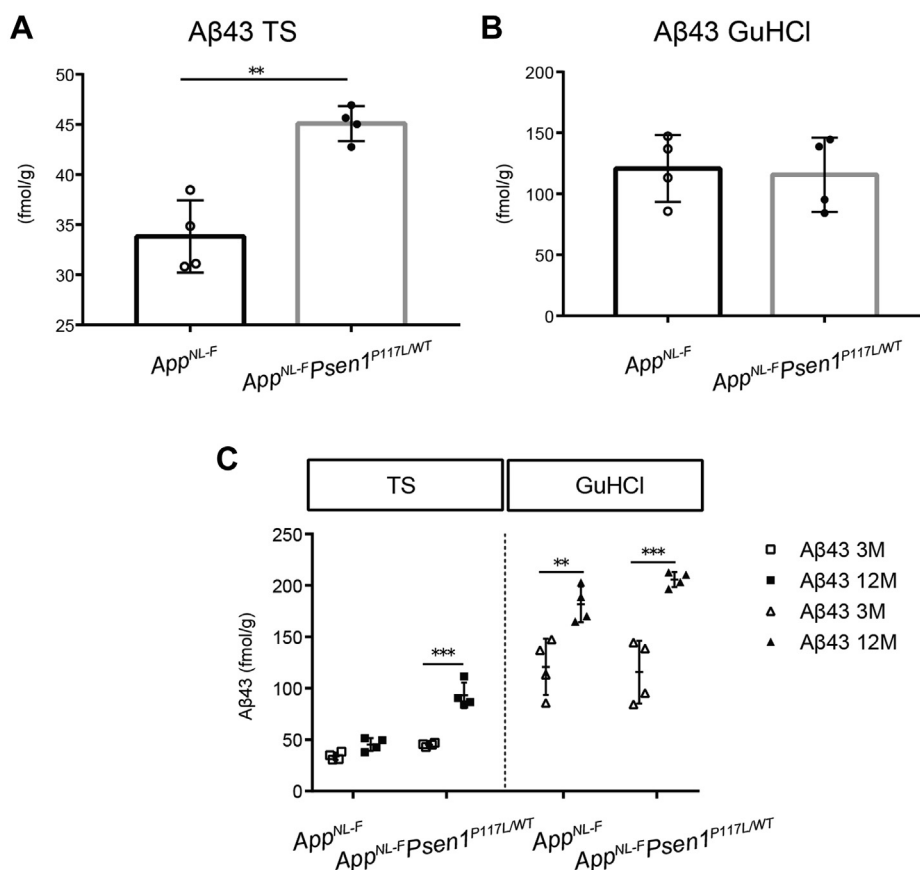


**Figure 2.**  $A\beta_{43}$  levels detected in the cortices of  $App^{NL-F}$  and  $App^{NL-F}Psen1^{P117L/WT}$  mice. A and B,  $A\beta_{43}$  quantified by ELISA using Tris-HCl (A) and GuHCl (B) soluble fractions from the cortices of 3-month-old  $App^{NL-F}$  and  $App^{NL-F}Psen1^{P117L/WT}$  mice.  $App^{NL-F}$  (n = 4) and  $App^{NL-F}Psen1^{P117L/WT}$  (n = 4) (Student's *t* test). C, quantity of  $A\beta_{43}$  from Tris-HCl and GuHCl soluble fractions from 3- and 12-month-old mice.  $App^{NL-F}$  (n = 4) and  $App^{NL-F}Psen1^{P117L/WT}$  (n = 4) (two-way ANOVA followed by Sidak's multiple comparisons test). Each bar represents mean  $\pm$  SD. \**p* < 0.05, \*\**p* < 0.01, \*\*\**p* < 0.001.

### Combination of the Swedish/Iberian and P117L mutations is associated with cored $A\beta$ plaque formation

Several lines of evidence support the notion that diversity in  $A\beta$  species correlates with plaque morphology such as typical cored plaques (35–37). We therefore performed costaining with N1D antibody raised against  $A\beta_{1-5}$  peptide (38) and 1-Fluoro-2,5-bis(3-carboxy-4-hydroxystyryl)benzene (FSB), which recognizes the  $\beta$ -sheet structure within amyloid fibrils and displays higher fluorescence intensity than 1-bromo-2, 5-bis-(3-hydroxycarbonyl-4-hydroxystyryl)benzene (BSB) and Congo red (39, 40). We observed that FSB-positive signals were positioned at the center of plaques (Fig. 4A) and that the N1D/FSB double-positive plaques were significantly increased in the cortex and hippocampus of  $App^{NL-F}Psen1^{P117L}$  mice compared with those of  $App^{NL-F}$  and  $App^{NL-G-F}$  mice (Fig. 4B). No significant difference was observed in the subcortical region between  $App^{NL-F}Psen1^{P117L}$  and  $App^{NL-G-F}$  mice. The frequent presence of classic dense-cored plaques in the cortex of double-mutant mice was confirmed by 3,3'-diaminobenzidine (DAB) staining (Fig. 4C).

### Neuroinflammation is elevated in $App^{NL-F}Psen1^{P117L}$ mice, particularly in the hippocampus

Neuroinflammation surrounding  $A\beta$  plaques manifests as one of the pathological features in AD patients (13, 41, 42), and genome-wide association studies (GWAS) have suggested

etiological involvement of neuroinflammation in AD development (43–45). We thus analyzed the neuroinflammatory status of three mouse lines ( $App^{NL-F}$ ,  $App^{NL-F}Psen1^{P117L}$ , and  $App^{NL-G-F}$ ) by immunofluorescence using antibodies against  $A\beta$  (82E1), microglia (Iba1), and astrocytes (anti-GFAP). We confirmed the presence of glial cells surrounding  $A\beta$  plaques in  $App^{NL-F}Psen1^{P117L}$  mice (Fig. 5, A and B). Consistent with our previous reports, single  $App^{NL-G-F}$  rather than  $App^{NL-F}$  mice exhibit robust microgliosis and astrocytosis accompanying progressive amyloidosis (13, 14). Quantification of immunofluorescence images indicated that more neuroinflammation was evident in  $App^{NL-F}Psen1^{P117L}$  and  $App^{NL-G-F}$  than  $App^{NL-F}$  mice (Fig. 5C). This was somewhat predictable because  $App^{NL-F}Psen1^{P117L}$  and  $App^{NL-G-F}$  mice accumulate more pathological  $A\beta$  than  $App^{NL-F}$  mice (Fig. 3, A–C). A unique observation is that  $App^{NL-F}Psen1^{P117L}$  mice exhibited significantly greater microgliosis and astrocytosis than  $App^{NL-G-F}$  mice in the hippocampus despite the indistinguishable levels of  $A\beta$  amyloidosis therein. This phenomenon may be associated with increased  $A\beta_{43}$  deposition (Fig. 3, D and E) and cored plaques in  $App^{NL-F}Psen1^{P117L}$  mice (Fig. 4, A and B), but these speculations alone cannot fully account for the neuroinflammation that took place selectively in the hippocampus. In any case, our findings indicate that  $App^{NL-F}Psen1^{P117L}$  mice may be suitable for investigating hippocampal neuroinflammation.

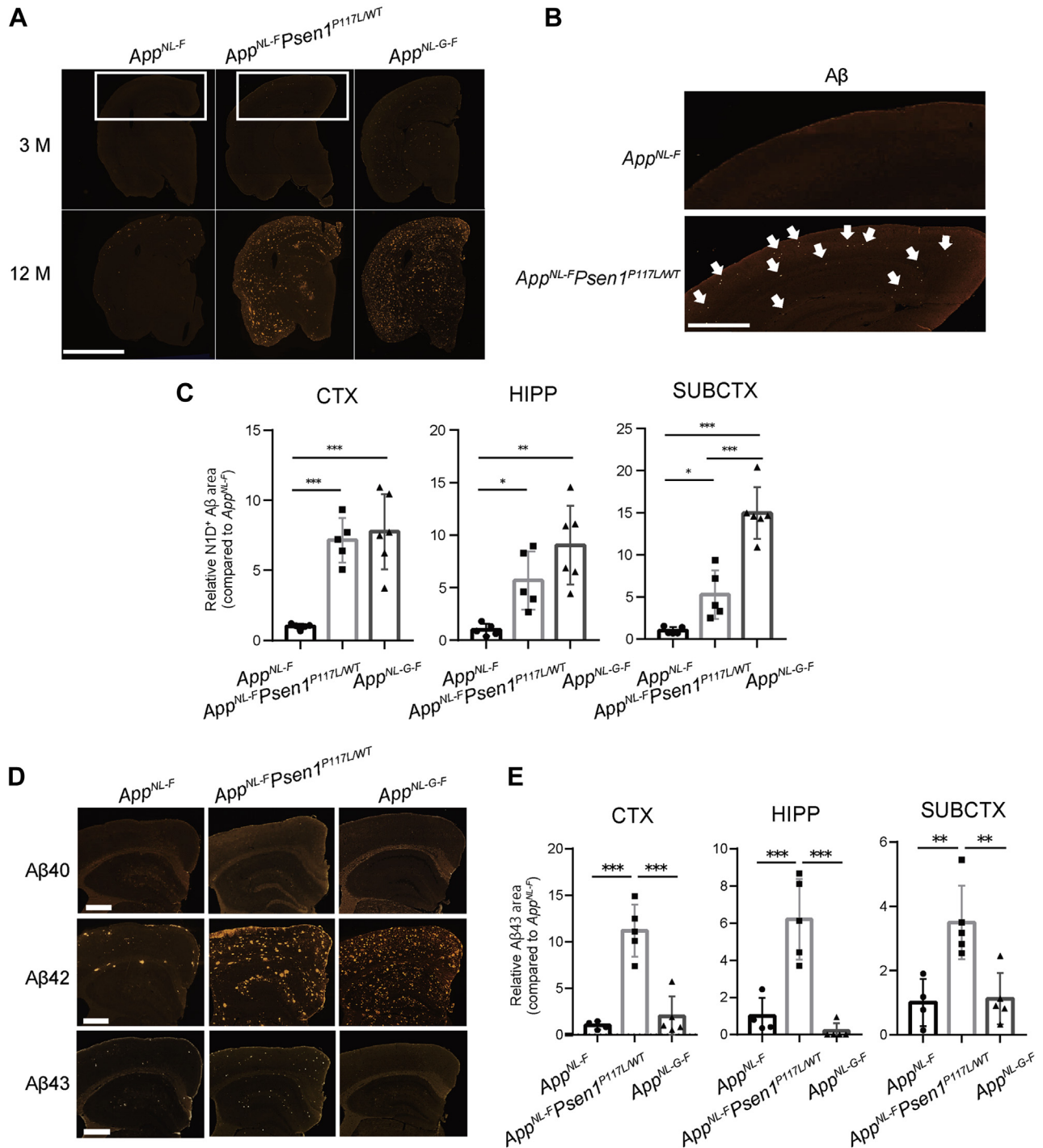


**Figure 3. A $\beta$  plaques deposited in the brains of *App<sup>NL-F</sup>Psen1<sup>P117L</sup>* mice.** *A*, immunofluorescence images showing amyloid pathology in the brains of 3- (top) and 12-month-old (bottom) *App<sup>NL-F</sup>*, *App<sup>NL-F</sup>Psen1<sup>P117L/WT</sup>* and *App<sup>NL-G-F</sup>* mice. Scale bar represents 2.5  $\mu$ m. *B*, high magnification images of tissue sections in (*A*) from 3-month-old animals. A $\beta$  deposition is indicated by white arrows. Scale bar represents 500  $\mu$ m. *C*, N1D-positive areas were quantified in cortical (CTX), hippocampal (HIPP), and subcortical (SUBCTX) regions, respectively. *App<sup>NL-F</sup>* ( $n = 5$ ), *App<sup>NL-F</sup>Psen1<sup>P117L/WT</sup>* ( $n = 5$ ) and *App<sup>NL-G-F</sup>* ( $n = 6$ ). *D*, sections from 12-month-old mice were immunostained with antibodies specific to A $\beta$ <sub>40</sub>, A $\beta$ <sub>42</sub>, and A $\beta$ <sub>43</sub>. Scale bars represent 50  $\mu$ m. *E*, quantification of A $\beta$ <sub>43</sub>-positive areas in cortical (CTX), hippocampal (HIPP), and subcortical (SUBCTX) regions of 12-month-old mice. *App<sup>NL-F</sup>* ( $n = 4$ ), *App<sup>NL-F</sup>Psen1<sup>P117L/WT</sup>* ( $n = 5$ ) and *App<sup>NL-G-F</sup>* ( $n = 5$ ) (one-way ANOVA followed by Tukey's multiple comparisons test). Each bar represents the mean  $\pm$  SD. \* $p < 0.05$ , \*\* $p < 0.01$ , \*\*\* $p < 0.001$ .

## Discussion

The primary aim of the present study was to generate *App* knock-in mice that pathologically accumulate wild-type human A $\beta$  devoid of the Arctic mutation. *App<sup>NL-G-F</sup>* mice carrying the

Arctic mutation exhibit the most rapid and aggressive pathology among all the *App* knock-in mice that had been created. Our motivation was based on the undesirable nature of the Arctic mutation that impedes the physiological metabolism and

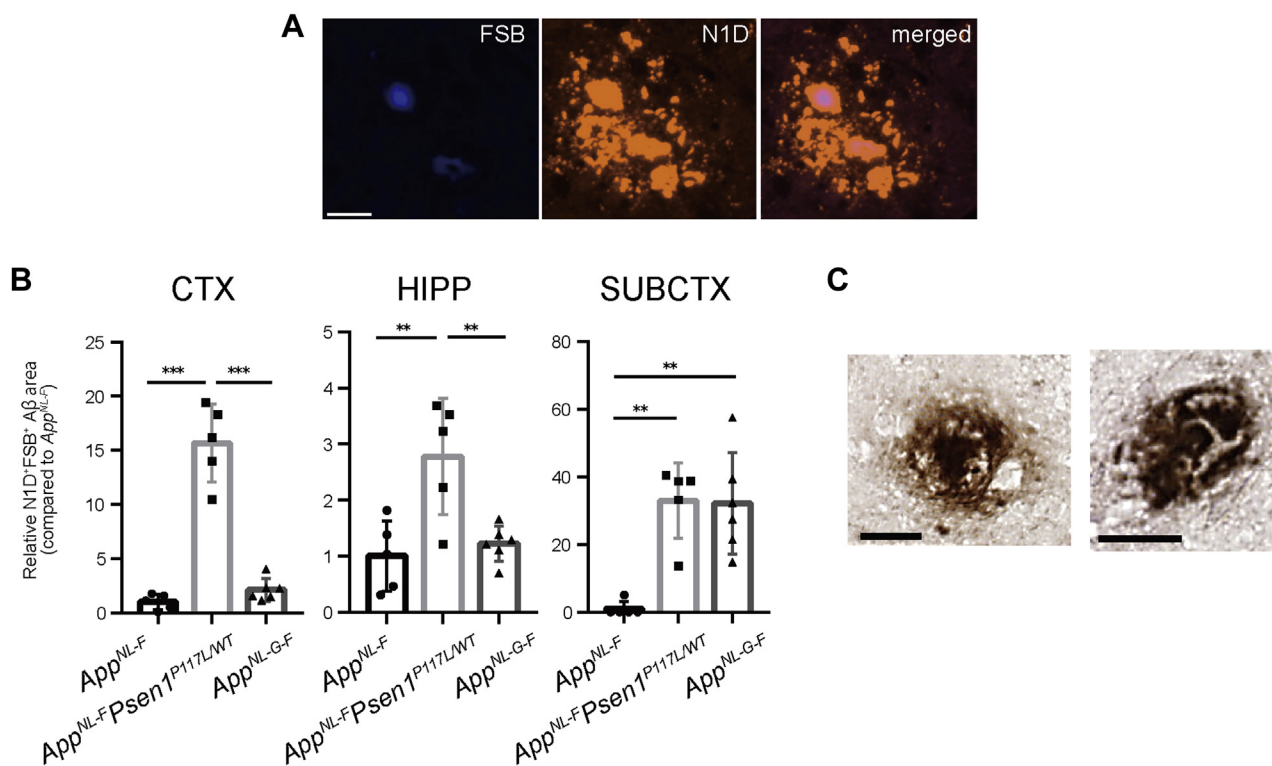


**Figure 4.** A $\beta$  plaques with a cored structure in  $App^{NL-F}Psen1^{P117L}$  mice. **A**, brain sections from 12-month-old  $App^{NL-F}Psen1^{P117L/WT}$  mice were costained with FSB and N1D antibody. **B**, FSB/N1D double-positive areas were quantified in the brains of  $App^{NL-F}$ ,  $App^{NL-F}Psen1^{P117L/WT}$ , and  $App^{NL-F}Psen1^{P117L/G-F}$  mice.  $App^{NL-F}$  (n = 5),  $App^{NL-F}Psen1^{P117L/WT}$  (n = 5), and  $App^{NL-F}Psen1^{P117L/G-F}$  (n = 6) (one-way ANOVA followed by Tukey's multiple comparisons test). Each bar represents mean  $\pm$  SD. \* $p < 0.05$ , \*\* $p < 0.01$ , \*\*\* $p < 0.001$ . **C**, representative images of dense-core plaques surrounded by a halo effect detected by DAB staining. Scale bars represent 25  $\mu$ m.

clearance of A $\beta$  (12, 25), thus making it difficult to study etiological processes upstream of A $\beta$  deposition. Arctic A $\beta$  also binds to anti-A $\beta$  antibodies raised against A $\beta$  peptide in a distinct manner (13), making  $App^{NL-G-F}$  mice unsuitable for preclinical immunotherapy studies. The generation of  $App$  knock-in mice that accumulate wild-type human A $\beta$  without the Arctic mutation as quickly as  $App^{NL-G-F}$  mice is therefore a prerequisite before disease-modifying strategies targeting mechanisms upstream of A $\beta$  deposition can be developed.

Introduction of the  $Psen1^{P117L}$  mutation into  $App^{NL-F}$  mice resulted in an unexpected acceleration of A $\beta_{42}$  and A $\beta_{43}$  deposition. Although the numbers of cortical and hippocampal plaques visualized by an antibody specific to the N-terminus of A $\beta$  (N1D) were indistinguishable between  $App^{NL-G-F}$  and  $App^{NL-F}Psen1^{P117L}$  mice,  $App^{NL-F}Psen1^{P117L}$  mice showed a larger number of cored plaques in the cortex and hippocampus and more gliosis in the hippocampus than was seen in  $App^{NL-G-F}$  mice. Mechanisms accounting for these observations are unclear but may be associated with the prion-like nature of A $\beta_{43}$  (46). In any case, the  $App^{NL-F}Psen1^{P117L}$  mice may become a useful tool for examining the roles of hippocampal neuroinflammation in the etiology of AD.

Other groups have also attempted to combine the  $App$  and  $Psen1$  mutations. Flood *et al.* (47) generated double knock-in mice that harbored the Swedish mutations in the  $App$  gene and the P264L/P264L mutation in the  $Psen1$  gene. These mice showed elevation of A $\beta_{42}$  levels and pathological amyloidosis without overexpression of APP. Although this model has seldom

been used in the research community presumably because the progression of pathology was too slow and mild, both their group and ours share similar ideas and goals. Similarly, Li *et al.* generated a mouse model of cerebral amyloid angiopathy (CAA) (48). We observed only a few CAA-like structures (less than ten per hemisphere) mainly in meninges in the 12-month-old  $App^{NL-F}Psen1^{P117L}$  mice, indicating that this is parenchymal amyloidosis-dominant model. Typical images of CAA are shown in Figure S3. Unlike the models generated by Flood *et al.* and Li *et al.*, our third-generation model mice are heterozygous for the  $Psen1$  mutation, making them easier to breed.

We must however point out that  $App^{NL-F}Psen1^{P117L}$  mice are probably inadequate for studying  $\beta$ - and  $\gamma$ -secretases and their modifiers because the cleavages catalyzed by these secretases are artificially altered by the mutations. We thus expect the mutant mice to become more suitable for the examining catabolism and clearance of A $\beta$  than its anabolism. This makes agonist(s) for somatostatin receptor subtype(s) a medication candidate for treatment of preclinical AD (49). We will share these mice with the AD research community to accelerate the fight against a disease that deprives patients of their human dignity.

## Materials and methods

### Animals

$App^{NL-F}$  and  $App^{NL-G-F}$  mice were described previously (13).  $Psen1^{P117L}$  mice (27) were crossed with the  $App^{NL-F}$  mice to generate  $App/Psen1$  double-mutant mice. All double-mutant

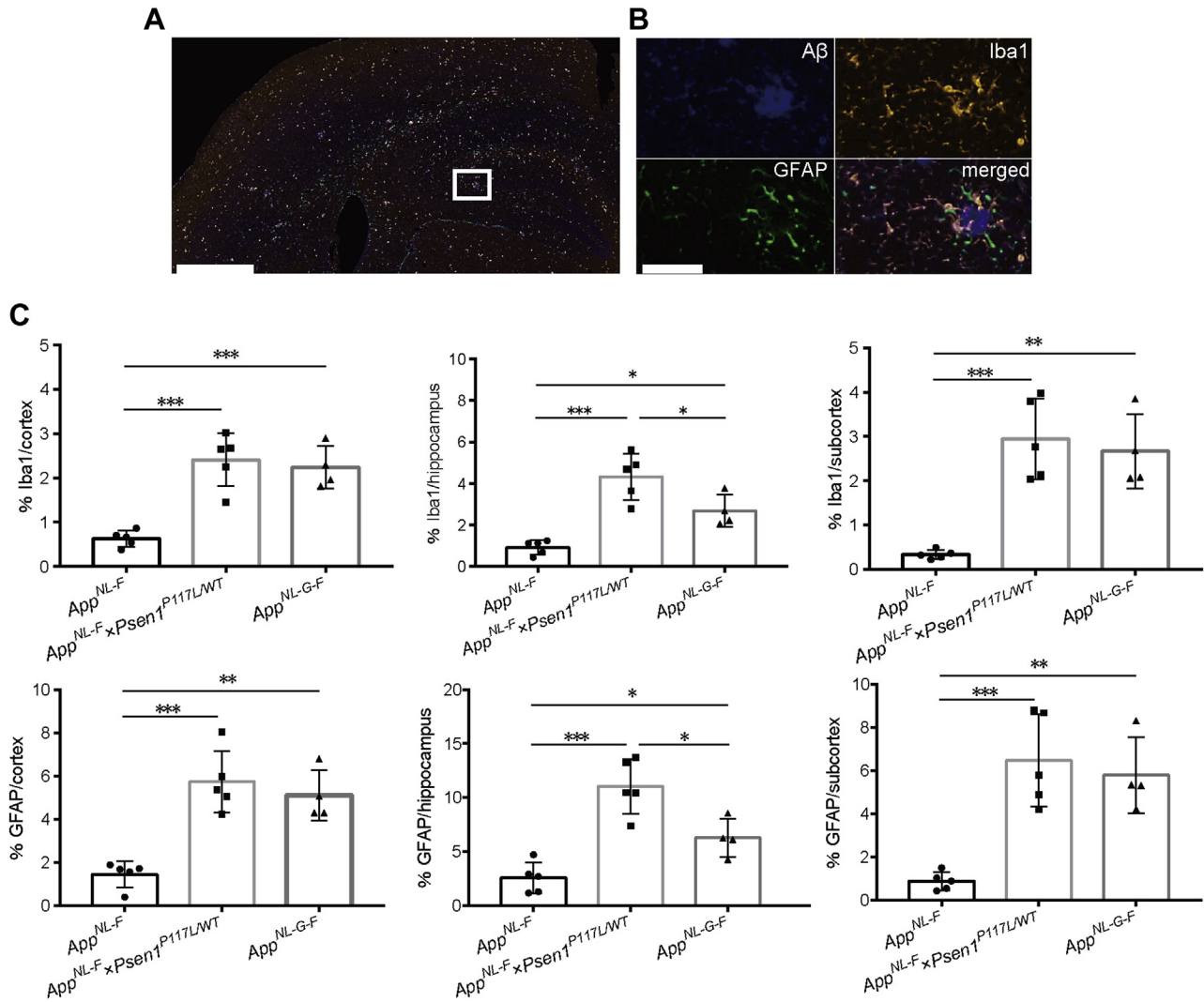


**Figure 5. Glial responses in  $App^{NL-F}Psen1^{P117L/WT}$  mouse brain.** A, inflammatory signals were detected with GFAP and Iba1 antibodies using brain sections from 12-month-old  $App^{NL-F}Psen1^{P117L/WT}$  mice.  $A\beta$  pathology was detected by immunostaining with 82E1 antibody. Scale bar represents 500  $\mu$ m. B, higher magnification image of the area marked in white in (A). Scale bar represents 50  $\mu$ m. C, immunoreactive areas of GFAP or Iba1 were quantified in the brains of  $App^{NL-F}$ ,  $App^{NL-F}Psen1^{P117L/WT}$  and  $App^{NL-G-F}$  mice. Each bar represents the mean  $\pm$  SD. \* $p$  < 0.05, \*\* $p$  < 0.01, \*\*\* $p$  < 0.001,  $App^{NL-F}$  ( $n$  = 5),  $App^{NL-F}Psen1^{P117L/WT}$  ( $n$  = 5), and  $App^{NL-G-F}$  ( $n$  = 4) (one-way ANOVA followed by Tukey's multiple comparisons test).

mice used in this study were homozygous for the *App* mutations and heterozygous for the *Psen1* mutation ( $App^{NL-F}Psen1^{P117L}$ ). C57BL/6J mice were used as controls. Male mice were used for biochemical analyses and both male and female mice were used for immunohistochemical studies. All mice were bred and maintained in accordance with regulations for animal experiments promulgated by the RIKEN Center for Brain Science.

### Genotyping

Genomic DNA was extracted from mouse tails in lysis buffer (10 mM pH 8.5 Tris-HCl, 5 mM pH 8.0 EDTA, 0.2% SDS, 200 mM NaCl, 20  $\mu$ g/ml proteinase K) and subjected to PCR, followed by Sanger sequencing analysis. Primers used for genotyping have been described previously (13, 27).

### Brain sample preparation

Mice were anesthetized with isoflurane, transcardially perfused, and fixed with 4% paraformaldehyde in PBS. The

brains were dissected on ice into two halves at the midline. One hemisphere was divided into several parts and stored at  $-80^{\circ}\text{C}$  for biochemical analysis, while the other was incubated at  $4^{\circ}\text{C}$  for 24 h and rinsed with PBS until paraffin processing for histochemical analysis.

### Western blotting

Mice brain tissues were homogenized in lysis buffer (50 mM Tris pH 7.6, 0.15 M NaCl, and Complete protease inhibitor cocktail [Roche]). Homogenates were incubated at  $4^{\circ}\text{C}$  for 1 h and centrifuged at 15,000 rpm for 30 min, and the supernatants were collected as loading samples. Equal amounts of proteins per lane were subjected to SDS-PAGE and transferred to PVDF or nitrocellulose membranes (Invitrogen). To detect APP-CTFs, delipidated samples were loaded and the membrane was boiled for 5 min in PBS before the next step. After washing and blocking at room temperature, the membranes were incubated at  $4^{\circ}\text{C}$  overnight with primary antibodies

## Improved model of Alzheimer's disease

against APP (1:1000, Millipore) or APP-CTFs (1:1000, Sigma-Aldrich) or against  $\beta$ -Actin as a loading control (1:5000, Sigma). The target protein on the membrane was visualized with ECL Select (GE Healthcare) and a Luminescent Image Analyzer LAS-3000 Mini (Fujifilm).

### Immunostaining

Paraffin-embedded mouse brain sections were subjected to deparaffinization and then antigen retrieval was performed by autoclave processing at 121 °C for 5 min. After inactivation of endogenous peroxidases using 0.3% H<sub>2</sub>O<sub>2</sub> solution for 30 min, the sections were washed with TNT buffer (0.1 M Tris pH 7.5, 0.15 M NaCl, 0.05% Tween20), blocked for 30 min in TNB buffer (0.1 M Tris pH 7.5, 0.15 M NaCl), and incubated in the same buffer with primary antibodies at 4 °C overnight. The primary antibody dilution ratios were as follows: A $\beta$ <sub>40</sub> (1:100, IBL), A $\beta$ <sub>42</sub> (1:100, IBL), A $\beta$ <sub>43</sub> (1:50, IBL), A $\beta$ 1-5 (N1D) (38) (1:200), N-terminus of A $\beta$  (82E1) (1:500, IBL), GFAP (1:200, Millipore), Iba1 (1:200, Wako), and  $\alpha$ -smooth muscle actin (1:1000, Sigma-Aldrich). Amyloid pathology was detected using biotinylated secondary antibody and tyramide signal amplification as described previously (50). For detection of glial activation and CAA, secondary antibodies conjugated with Alexa Fluor 488 or 555 were used. Before mounting, the sections were treated when necessary with Hoechst33342 diluted in PBS. Data images were obtained using a NanoZoomer Digital Pathology C9600 (Hamamatsu Photonics) and EVOS M5000 Imaging System (Thermo Fisher scientific). Immunoreactive signals were quantified by Definiens Tissue Studio (Definiens).

### DAB staining

Targeted signals were detected and visualized using VEC-TASTAIN *Elite* ABC Rabbit IgG kit (Funakoshi) and DAB·TRIS tablets (Mutokagaku). After deparaffinization and antigen retrieval treatment of mouse brain sections, endogenous peroxidases were inactivated using 0.3% H<sub>2</sub>O<sub>2</sub> solution for 30 min. The sections were blocked with three drops of goat serum in PBS for 30 min at room temperature and incubated with N1D antibody at 4 °C overnight. The sections were washed with PBS and incubated with the *Elite* ABC solution for 30 min and subsequently stained with DAB solution following the manufacturer's instructions. Before mounting, dehydration treatment was performed.

### FSB staining

The PFA-fixed tissue sections were deparaffinized, incubated in 0.01% FSB solution in EtOH for 30 min, and then rinsed in saturated Li<sub>2</sub>CO<sub>3</sub> in water for 15–20 s at room temperature. The sections were differentiated in EtOH for 3 min followed by immersion in water for 5 min to stop the reaction. Readers should refer to the [Immunostaining](#) section concerning methods for subsequent treatments following antigen retrieval.

### ELISA

Mouse cortical samples were homogenized in buffer A (50 mM Tris-HCl, pH 7.6, 150 mM NaCl, and protease

inhibitor cocktail) using a medical beads shocker. The homogenized samples were directed to centrifugation at 70,000 rpm for 20 min at 4 °C, and the supernatant was measured and collected as a Tris-soluble (TS) fraction in 6 M guanidine-HCl (Gu-HCl) solution containing 50 mM Tris and protease inhibitors. The pellet was loosened with the buffer A and centrifuged at 70,000 rpm for 5 min at 4 °C, and then dissolved in 6 M Gu-HCl buffer. After incubation at room temperature for 1 h, the sample was sonicated at 25 °C for 1 min. Subsequently, the sample was centrifuged at 70,000 rpm for 20 min at 25 °C and the supernatant collected as a Gu-HCl fraction. 100  $\mu$ l of TS and Gu-HCl fractions were loaded onto 96-well plates and incubated at 4 °C overnight using the A $\beta$ <sub>40</sub>, A $\beta$ <sub>42</sub> and A $\beta$ <sub>43</sub> ELISA kit (Wako) according to the manufacturer's instructions.

### Statistics

All data are presented as the mean  $\pm$  SD within each figure. For comparisons between two groups, data were analyzed by Student's *t* test. For comparisons among more than three groups, we used one-way analysis of variance (ANOVA) followed by Tukey's multiple comparisons test. Two-way ANOVA followed by Sidak's multiple comparisons test were used when two data sets were analyzed. Statistical analyses were performed using GraphPad Prism version 7.00 software (GraphPad software). The levels of statistical significance were shown as *p*-values: \**p* < 0.05, \*\**p* < 0.01, \*\*\**p* < 0.001.

### Data availability

Data will be shared upon request at [takaomi.saido@riken.jp](mailto:takaomi.saido@riken.jp) or [hiroki.sasaguri@riken.jp](mailto:hiroki.sasaguri@riken.jp).

*Supporting information*—This article contains [supporting information](#).

*Acknowledgments*—We thank Yukiko Nagai-Watanabe for secretarial work.

*Author contributions*—K. S., N. W., R. F., K. N., T. O., T. S., T. C. S., and H. S. conceptualization; K. S., N. W., R. F., N. M., M. S., K. N., and H. S. data curation; K. S., N. W., R. F., T. O., T. S., T. C. S., and H. S. formal analysis; K. S., N. W., and T. C. S. funding acquisition; K. S., N. W., R. F., N. M., M. S., K. N., T. O., T. S., T. C. S., and H. S. investigation; K. S., N. W., R. F., N. M., M. S., K. N., T. O., T. S., T. C. S., and H. S. methodology; K. S., N. W., T. C. S., and H. S. project administration; K. S., N. W., R. F., M. S., K. N., T. S., T. C. S., and H. S. resources; K. S., N. W., R. F., N. M., M. S., T. S., and T. C. S. software; K. S., N. W., T. O., T. S., T. C. S., and H. S. supervision; K. S., N. W., R. F., K. N., T. O., T. S., T. C. S., and H. S. validation; K. S., N. W., R. F. and H. S. visualization; K. S., N. W., R. F., T. C. S., and H. S. writing-original draft.

*Funding and additional information*—This work was supported by AMED under Grant Number JP20dm0207001 (Brain Mapping by Integrated Neurotechnologies for Disease Studies (Brain/MINDS)) (T. C. S.) and JSPS KAKENHI Grant Number JP18K07402 (H. S.).



**Conflicts of interest**—The authors declare that they have no conflicts of interest with the contents of this article.

**Abbreviations**—The abbreviations used are: A $\beta$ , amyloid  $\beta$  peptide; AD, Alzheimer's disease; AICD, APP intracellular domain; ANOVA, one-way analysis of variance; APP, amyloid precursor protein; BSB, 1-bromo-2,5-bis-(3-hydroxycarbonyl-4-hydroxystyryl) benzene; CAA, cerebral amyloid angiopathy; DAB, 3,3'-diaminobenzidine; ELISA, Enzyme-Linked Immunosorbent Assay; FSB, 1-Fluoro-2,5-bis(3-carboxy-4-hydroxystyryl)benzene; GuHCl, guanidine hydrochloride; GWAS, genome-wide association studies; PSEN, presenilin.

## References

- Selkoe, D. J., and Hardy, J. (2016) The amyloid hypothesis of Alzheimer's disease at 25 years. *EMBO Mol. Med.* **8**, 595–608
- Karran, E., and De Strooper, B. (2016) The amyloid cascade hypothesis: Are we poised for success or failure? *J. Neurochem.* **139 Suppl 2**, 237–252
- Sasaguri, H., Nilsson, P., Hashimoto, S., Nagata, K., Saito, T., De Strooper, B., Hardy, J., Vassar, R., Winblad, B., and Saido, T. C. (2017) APP mouse models for Alzheimer's disease preclinical studies. *EMBO J.* **36**, 2473–2487
- Kwart, D., Gregg, A., Scheckel, C., Murphy, E. A., Paquet, D., Duffield, M., Fak, J., Olsen, O., Darnell, R. B., and Tessier-Lavigne, M. (2019) A large panel of isogenic APP and PSEN1 mutant human iPSC neurons reveals shared endosomal abnormalities mediated by APP  $\beta$ -CTFs, not A $\beta$ . *Neuron* **104**, 256–270.e255
- Nalivaeva, N. N., Belyaev, N. D., Kerridge, C., and Turner, A. J. (2014) Amyloid-clearing proteins and their epigenetic regulation as a therapeutic target in Alzheimer's disease. *Front. Aging Neurosci.* **6**, 235
- Saito, T., Matsuba, Y., Yamazaki, N., Hashimoto, S., and Saido, T. C. (2016) Calpain activation in Alzheimer's model mice is an artifact of APP and presenilin overexpression. *J. Neurosci.* **36**, 9933–9936
- Higuchi, M., Iwata, N., Matsuba, Y., Takano, J., Suemoto, T., Maeda, J., Ji, B., Ono, M., Staufenbiel, M., Suhara, T., and Saido, T. C. (2012) Mechanistic involvement of the calpain-calpastatin system in Alzheimer neuropathology. *FASEB J.* **26**, 1204–1217
- Hashimoto, S., Ishii, A., Kamano, N., Watamura, N., Saito, T., Ohshima, T., Yokosuka, M., and Saido, T. C. (2018) Endoplasmic reticulum stress responses in mouse models of Alzheimer's disease: Overexpression paradigm versus knockin paradigm. *J. Biol. Chem.* **293**, 3118–3125
- Gamache, J., Benzow, K., Forster, C., Kemper, L., Hlynialuk, C., Furrow, E., Ashe, K. H., and Koob, M. D. (2019) Factors other than hTau overexpression that contribute to tauopathy-like phenotype in rTg4510 mice. *Nat. Commun.* **10**, 2479
- Citron, M., Oltsersdorf, T., Haass, C., McConlogue, L., Hung, A. Y., Seubert, P., Vigo-Pelfrey, C., Lieberburg, I., and Selkoe, D. J. (1992) Mutation of the beta-amyloid precursor protein in familial Alzheimer's disease increases beta-protein production. *Nature* **360**, 672–674
- Lichtenthaler, S. F., Wang, R., Grimm, H., Uljon, S. N., Masters, C. L., and Beyreuther, K. (1999) Mechanism of the cleavage specificity of Alzheimer's disease gamma-secretase identified by phenylalanine-scanning mutagenesis of the transmembrane domain of the amyloid precursor protein. *Proc. Natl. Acad. Sci. U. S. A.* **96**, 3053–3058
- Nilsberth, C., Westlind-Danielsson, A., Eckman, C. B., Condron, M. M., Axelman, K., Forsell, C., Stenh, C., Luthman, J., Teplow, D. B., Younkin, S. G., Näslund, J., and Lannfelt, L. (2001) The 'Arctic' APP mutation (E693G) causes Alzheimer's disease by enhanced Abeta protofibril formation. *Nat. Neurosci.* **4**, 887–893
- Saito, T., Matsuba, Y., Mihira, N., Takano, J., Nilsson, P., Itohara, S., Iwata, N., and Saido, T. C. (2014) Single App knock-in mouse models of Alzheimer's disease. *Nat. Neurosci.* **17**, 661–663
- Masuda, A., Kobayashi, Y., Kogo, N., Saito, T., Saido, T. C., and Itohara, S. (2016) Cognitive deficits in single App knock-in mouse models. *Neurobiol. Learn Mem.* **135**, 73–82
- Shirotani, K., Hori, Y., Yoshizaki, R., Higuchi, E., Colonna, M., Saito, T., Hashimoto, S., Saito, T., Saido, T. C., and Iwata, N. (2019) Amino-phospholipids are signal-transducing TREM2 ligands on apoptotic cells. *Sci. Rep.* **9**, 7508
- Chen, W. T., Lu, A., Craessaerts, K., Pavie, B., Sala Frigerio, C., Corthout, N., Qian, X., Laláková, J., Kühnemund, M., Voytyuk, I., Wolfs, L., Mancuso, R., Salta, E., Balusu, S., Snellinx, A., et al. (2020) Spatial transcriptomics and in situ sequencing to study Alzheimer's disease. *Cell* **182**, 976–991.e919
- Sobue, A., Komine, O., Hara, Y., Endo, F., Mizoguchi, H., Watanabe, S., Murayama, S., Saito, T., Saido, T. C., Sahara, N., Higuchi, M., Ogi, T., and Yamanaka, K. (2021) Microglial gene signature reveals loss of homeostatic microglia associated with neurodegeneration of Alzheimer's disease. *Acta Neuropathol. Commun.* **9**, 1
- Nortley, R., Korte, N., Izquierdo, P., Hirunpattarasilp, C., Mishra, A., Jaunmuktane, Z., Kyrargyri, V., Pfeiffer, T., Khenouf, L., Madry, C., Gong, H., Richard-Loendt, A., Huang, W., Saito, T., Saido, T. C., et al. (2019) Amyloid  $\beta$  oligomers constrict human capillaries in Alzheimer's disease via signaling to pericytes. *Science* **365**, eaav9518
- Hashimoto, S., Matsuba, Y., Kamano, N., Mihira, N., Sahara, N., Takano, J., Muramatsu, S. I., Saido, T. C., and Saito, T. (2019) Tau binding protein CAPON induces tau aggregation and neurodegeneration. *Nat. Commun.* **10**, 2394
- Hongo, N., Takamura, Y., Nishimaru, H., Matsumoto, J., Tobe, K., Saito, T., Saido, T. C., and Nishijo, H. (2020) Astaxanthin ameliorated parvalbumin-positive neuron deficits and Alzheimer's disease-related pathological progression in the Hippocampus of App(NL-G-F/NL-G-F) mice. *Front. Pharmacol.* **11**, 307
- Uruno, A., Matsumaru, D., Ryoike, R., Saito, R., Kadoguchi, S., Saigusa, D., Saito, T., Saido, T. C., Kawashima, R., and Yamamoto, M. (2020) Nrf2 suppresses oxidative stress and inflammation in App knock-in Alzheimer's disease model mice. *Mol. Cell Biol.* **40**, e00467-19
- Saito, T., Mihira, N., Matsuba, Y., Sasaguri, H., Hashimoto, S., Narasimhan, S., Zhang, B., Murayama, S., Higuchi, M., Lee, V. M. Y., Trojanowski, J. Q., and Saido, T. C. (2019) Humanization of the entire murine Mapt gene provides a murine model of pathological human tau propagation. *J. Biol. Chem.* **294**, 12754–12765
- Jun, H., Bramian, A., Soma, S., Saito, T., Saido, T. C., and Igarashi, K. M. (2020) Disrupted place cell remapping and impaired grid cells in a knockin model of Alzheimer's disease. *Neuron* **107**, 1095–1112.e1096
- Sutoko, S., Masuda, A., Kandori, A., Sasaguri, H., Saito, T., Saido, T. C., and Funane, T. (2021) Early identification of Alzheimer's disease in mouse models: Application of deep neural network algorithm to cognitive behavioral parameters. *iScience* **24**, 102198
- Tsubuki, S., Takaki, Y., and Saido, T. C. (2003) Dutch, Flemish, Italian, and Arctic mutations of APP and resistance of Abeta to physiologically relevant proteolytic degradation. *Lancet* **361**, 1957–1958
- Morishima-Kawashima, M., Oshima, N., Ogata, H., Yamaguchi, H., Yoshimura, M., Sugihara, S., and Ihara, Y. (2000) Effect of apolipoprotein E allele epsilon4 on the initial phase of amyloid beta-protein accumulation in the human brain. *Am. J. Pathol.* **157**, 2093–2099
- Sasaguri, H., Nagata, K., Sekiguchi, M., Fujioka, R., Matsuba, Y., Hashimoto, S., Sato, K., Kurup, D., Yokota, T., and Saido, T. C. (2018) Introduction of pathogenic mutations into the mouse Psen1 gene by base editor and target-AID. *Nat. Commun.* **9**, 2892
- Komor, A. C., Kim, Y. B., Packer, M. S., Zuris, J. A., and Liu, D. R. (2016) Programmable editing of a target base in genomic DNA without double-stranded DNA cleavage. *Nature* **533**, 420–424
- Saito, T., Suemoto, T., Brouwers, N., Slegers, K., Funamoto, S., Mihira, N., Matsuba, Y., Yamada, K., Nilsson, P., Takano, J., Nishimura, M., Iwata, N., Van Broeckhoven, C., Ihara, Y., and Saido, T. C. (2011) Potent amyloidogenicity and pathogenicity of A $\beta$ 43. *Nat. Neurosci.* **14**, 1023–1032
- Saido, T. C., and Iwata, N. (2006) Metabolism of amyloid beta peptide and pathogenesis of Alzheimer's disease. Towards presymptomatic diagnosis, prevention and therapy. *Neurosci. Res.* **54**, 235–253
- Shimojo, M., Sahara, N., Mizoroki, T., Funamoto, S., Morishima-Kawashima, M., Kudo, T., Takeda, M., Ihara, Y., Ichinose, H., and Takashima, A.

- (2008) Enzymatic characteristics of I213T mutant presenilin-1/gamma-secretase in cell models and knock-in mouse brains: Familial Alzheimer disease-linked mutation impairs gamma-site cleavage of amyloid precursor protein C-terminal fragment beta. *J. Biol. Chem.* **283**, 16488–16496
32. Takami, M., Nagashima, Y., Sano, Y., Ishihara, S., Morishima-Kawashima, M., Funamoto, S., and Ihara, Y. (2009) gamma-Secretase: successive tripeptide and tetrapeptide release from the transmembrane domain of beta-carboxyl terminal fragment. *J. Neurosci.* **29**, 13042–13052
  33. Qi-Takahara, Y., Morishima-Kawashima, M., Tanimura, Y., Dolios, G., Hirotani, N., Horikoshi, Y., Kametani, F., Maeda, M., Saido, T. C., Wang, R., and Ihara, Y. (2005) Longer forms of amyloid beta protein: Implications for the mechanism of intramembrane cleavage by gamma-secretase. *J. Neurosci.* **25**, 436–445
  34. Thal, D. R., Rüb, U., Orantes, M., and Braak, H. (2002) Phases of A beta-deposition in the human brain and its relevance for the development of AD. *Neurology* **58**, 1791–1800
  35. Boon, B. D. C., Bulk, M., Jonker, A. J., Morrema, T. H. J., van den Berg, E., Popovic, M., Walter, J., Kumar, S., van der Lee, S. J., Holstege, H., Zhu, X., Van Nostrand, W. E., Natte, R., van der Weerd, L., Bouwman, F. H., *et al.* (2020) The coarse-grained plaque: A divergent Aβ42 plaque-type in early-onset Alzheimer's disease. *Acta Neuropathol.* **140**, 811–830
  36. Fukumoto, H., Asami-Odaka, A., Suzuki, N., Shimada, H., Ihara, Y., and Iwatsubo, T. (1996) Amyloid beta protein deposition in normal aging has the same characteristics as that in Alzheimer's disease. Predominance of A beta 42(43) and association of A beta 40 with cored plaques. *Am. J. Pathol.* **148**, 259–265
  37. Iwatsubo, T., Odaka, A., Suzuki, N., Mizusawa, H., Nukina, N., and Ihara, Y. (1994) Visualization of A beta 42(43) and A beta 40 in senile plaques with end-specific A beta monoclonals: Evidence that an initially deposited species is A beta 42(43). *Neuron* **13**, 45–53
  38. Saido, T. C., Yokota, M., Maruyama, K., Yamao-Harigaya, W., Tani, E., Ihara, Y., and Kawashima, S. (1994) Spatial resolution of the primary beta-amyloidogenic process induced in postischemic hippocampus. *J. Biol. Chem.* **269**, 15253–15257
  39. Sato, K., Higuchi, M., Iwata, N., Saido, T. C., and Sasamoto, K. (2004) Fluoro-substituted and <sup>13</sup>C-labeled styrylbenzene derivatives for detecting brain amyloid plaques. *Eur. J. Med. Chem.* **39**, 573–578
  40. Higuchi, M., Iwata, N., Matsuba, Y., Sato, K., Sasamoto, K., and Saido, T. C. (2005) 19F and 1H MRI detection of amyloid beta plaques *in vivo*. *Nat. Neurosci.* **8**, 527–533
  41. Heneka, M. T., Carson, M. J., El Khoury, J., Landreth, G. E., Brosseron, F., Feinstein, D. L., Jacobs, A. H., Wyss-Coray, T., Vitorica, J., Ransohoff, R. M., Herrup, K., Frautschy, S. A., Finsen, B., Brown, G. C., Verkhratsky, A., *et al.* (2015) Neuroinflammation in Alzheimer's disease. *Lancet Neurol.* **14**, 388–405
  42. Nicoll, J. A., Wilkinson, D., Holmes, C., Steart, P., Markham, H., and Weller, R. O. (2003) Neuropathology of human Alzheimer disease after immunization with amyloid-beta peptide: A case report. *Nat. Med.* **9**, 448–452
  43. Lewcock, J. W., Schlepckow, K., Di Paolo, G., Tahirovic, S., Monroe, K. M., and Haass, C. (2020) Emerging microglia biology defines novel therapeutic Approaches for Alzheimer's disease. *Neuron* **108**, 801–821
  44. Podleśny-Drabiniok, A., Marcora, E., and Goate, A. M. (2020) Microglial phagocytosis: A disease-associated process emerging from Alzheimer's disease genetics. *Trends Neurosci.* **43**, 965–979
  45. Qin, Q., Teng, Z., Liu, C., Li, Q., Yin, Y., and Tang, Y. (2021) TREM2, microglia, and Alzheimer's disease. *Mech. Ageing Dev.* **195**, 111438
  46. Ruiz-Riquelme, A., Mao, A., Barghash, M. M., Lau, H. H. C., Stuart, E., Kovacs, G. G., Nilsson, K. P. R., Fraser, P. E., Schmitt-Ulms, G., and Watts, J. C. (2021) Aβ43 aggregates exhibit enhanced prion-like seeding activity in mice. *Acta Neuropathol. Commun.* **9**, 83
  47. Flood, D. G., Reaume, A. G., Dorfman, K. S., Lin, Y. G., Lang, D. M., Trusko, S. P., Savage, M. J., Annaert, W. G., De Strooper, B., Siman, R., and Scott, R. W. (2002) FAD mutant PS-1 gene-targeted mice: increased A beta 42 and A beta deposition without APP overproduction. *Neurobiol. Aging* **23**, 335–348
  48. Li, H., Guo, Q., Inoue, T., Polito, V. A., Tabuchi, K., Hammer, R. E., Pautler, R. G., Taffet, G. E., and Zheng, H. (2014) Vascular and parenchymal amyloid pathology in an Alzheimer disease knock-in mouse model: Interplay with cerebral blood flow. *Mol. Neurodegener.* **9**, 28
  49. Saito, T., Iwata, N., Tsubuki, S., Takaki, Y., Takano, J., Huang, S. M., Suemoto, T., Higuchi, M., and Saido, T. C. (2005) Somatostatin regulates brain amyloid beta peptide Abeta42 through modulation of proteolytic degradation. *Nat. Med.* **11**, 434–439
  50. Enya, M., Morishima-Kawashima, M., Yoshimura, M., Shinkai, Y., Kusui, K., Khan, K., Games, D., Schenk, D., Sugihara, S., Yamaguchi, H., and Ihara, Y. (1999) Appearance of sodium dodecyl sulfate-stable amyloid beta-protein (Aβ42) dimer in the cortex during aging. *Am. J. Pathol.* **154**, 271–279